Journal of Solid State Chemistry **150,** 104–111 (2000)
doi:10.1006/jssc.1999.8554, available online at http://www.idealibrary.com on IDEAL®

Investigation of $K_2MnF_5 \cdot H_2O$ by Neutron Diffraction

T. Roisnel,*,[1] P. Núñez,†,[2] A. Tressaud,‡ E. Molins,§ and J. Rodríguez-Carvajal*

Laboratoire Léon Brillouin (CEA-CNRS), CEA-Saclay, 91191 Gif-sur-Yvette Cedex, France; †Departamento de Química Inorgánica, Universidad de La Laguna, E-38200 La Laguna, Tenerife, Spain; ‡ICMCB, Université de Bordeaux I, Av. Dr. A. Schweitzer, 33608 Pessac Cedex, France; §ICMAB, Campus de la UAB, 08193 Bellaterra, Spain

Received August 4, 1999; in revised form October 14, 1999; accepted October 22, 1999

Crystal and magnetic structures of the chain pentafluoromanganate $K_2MnF_5 \cdot H_2O$ have been investigated by means of neutron powder diffraction. Neutron data recorded in the paramagnetic state are consistent with the monoclinic $P2_1/m$ space group and have allowed us to confirm a previously proposed structural model with $a < c$. $K_2MnF_5 \cdot H_2O$ orders antiferromagnetically below $T_N = 16.2$ K (propagation vector k = (0 0 ½)) and the magnetic structure can be described by antiferromagnetic chains coupled in a ferromagnetic manner along a and antiferromagnetically along c. The magnetic moment of Mn^{3+} ions is found to be equal to 3.1(1) μ_B at 1.5 K. We have determined the conditions to be satisfied by the isotropic exchange integrals in order to obtain the observed magnetic structure as the ground state.

Key Words: **manganese(III); fluoride; one-dimensional antiferromagnetism; magnetic structure; neutron diffraction; $K_2MnF_5 \cdot H_2O$.**

INTRODUCTION

The chemistry of fluoromanganates(III) has been studied with great interest during the last decade. Investigations have been especially focused on their structural and magnetic properties (1–10), but also on their spectroscopic properties (11–13). In previous studies we have emphasized the tendency of these compounds to form chains or layers of corner-shared $[MnF_6]$ octahedra. The low-dimensionality feature of these fluorides is intimately related to the Jahn–Teller effect, which arises from the high-spin d^4 configuration of the Mn(III).

In the case of $A_2MnF_5 \cdot xH_2O$ ($x = 0, 1$) linear-chain compounds, it has been found that the magnetic properties are strongly dependent on the structural features, in particular on the intrachain Mn–F–Mn angles (2). In previous papers, the magnetic structures of $A_2MnF_5 \cdot xH_2O$ compounds (A = Li(14), Na(8a), Rb(8b), Tl(4)) have been reported. The neutron powder diffraction studies have confirmed that all compounds contain antiferromagnetic chains and have clearly shown that interchain magnetic couplings are strongly dependent on both the nature of the monovalent cation and the water content.

This systematic study is here completed with the investigation of the $K_2MnF_5 \cdot H_2O$ compound. Although its crystal structure seemed to be well established, some discrepancies remained in the proposed cell parameters. We shall explain in this article the origin of this inconsistency.

The magnetic properties of $K_2MnF_5 \cdot H_2O$ together with those of several other pentafluoromanganates(III), have been investigated (1, 2, 6). These pentafluoromanganates have a one-dimensional antiferromagnetic behavior, and their magnetic exchange constant, J/k, has been determined by fitting the magnetic susceptibility data to Fisher's equation (15) adapted by Smith and Friedberg (16) for finite chains with $S = 2$. The calculated values of J/k for these compounds have been correlated with the intrachain Mn–F–Mn angles and Mn–Mn distances (1). In the case of $K_2MnF_5 \cdot H_2O$, the susceptibility measurements lead to a Néel temperature of 17.6 K (6).

EXPERIMENTAL

Sample Preparation

A solution of Mn_2O_3 dissolved in hot hydrofluoric acid (2 N) was mixed with an aqueous solution of KF in the molar ratio 1:10. Both solutions were mixed at room temperature in order to avoid the formation of the brown $KMnF_4 \cdot H_2O$ phase; a pink precipitate appeared within a few minutes. This method, which was different to those previously described (17, 18), led to pure $K_2MnF_5 \cdot H_2O$ compound. Single crystals could be grown from the mother liquor by very slow evaporation (1–2 weeks).

[1]Present address: Laboratoire de Chimie du Solide et Inorganique Moleculaire (UMR6511), Université de Rennes I, 35042 Rennes Cedex, France.

[2]To whom correspondence should be addressed. Fax: +34 922 318461. E-mail: pnunez@ull.es.

0022-4596/00 $35.00

TGA

TGA experiments were carried out on powdered samples under both vacuum and Ar flow. The weight loss confirmed the presence of one water molecule per formula. Similar results were previously found by IR spectroscopy (19).

Neutron Diffraction Experiments

Neutron diffraction measurements were performed at the Orphée reactor (Saclay, France) of the LLB, on the G4.1 ($\lambda = 2.426$ Å) diffractometer (20) for the determination of the magnetic structure in the temperature range 1.5–27 K and on the G4.2 diffractometer ($\lambda = 3.1308$ Å) (2θ range, 25°–145°) for the cell parameter measurements in the temperature range 25–295 K. A neutron diffraction pattern has also been recorded on the High-Resolution Multicounter Powder Diffractometer recently installed at the G4.2 site ($\lambda = 2.3433$ Å), in order to localize the atomic positions of water molecules at low temperature, $T = 30$ K (Fig. 1). Neutron data were analyzed with the Rietveld method using the program FullProf (21). The neutron scattering lengths and magnetic form factor of Mn^{3+}, stored in the program, are taken from Refs. (22) and (23), respectively.

RESULTS AND DISCUSSION

Nuclear Structure of $K_2MnF_5 \cdot H_2O$

The crystal structure of $K_2MnF_5 \cdot H_2O$ has been determined at room temperature (7, 18) and consists of infinite chains of [MnF_6] distorted octahedra running parallel to the monoclinic **b** axis. A phase transition has also been found at 81°C: $K_2MnF_5 \cdot H_2O$ has a monoclinic symmetry at room temperature ($P2_1/m$, $a = 6.112(1)$ Å; $b = 8.210(2)$ Å; $c = 5.994(1)$ Å; $\beta = 97.01°$), whereas above 81°C it transforms into a structure with orthorhombic symmetry (*Cmcm*, $a = 9.123(2)$ Å; $b = 8.002(1)$ Å; $c = 8.217(2)$ Å) (24). The orthorhombic parameters are very close to those of analogous compounds $Rb_2MnF_5 \cdot H_2O$ (25) and $Cs_2MnF_5 \cdot H_2O$ (26) at room temperature.

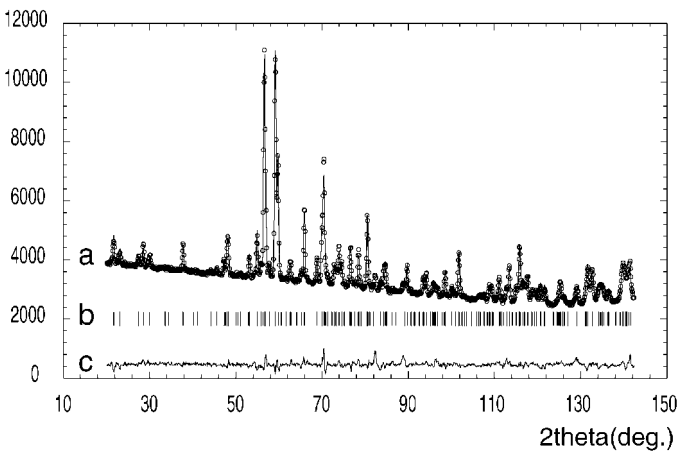

FIG. 1. Neutron diffraction patterns of $K_2MnF_5 \cdot H_2O$ collected at 30 K in the high-resolution neutron diffractometer G4.2 at LLB: (a) Experimental (circles) and calculated (continuous line) profiles; (b) vertical ticks for 2θ Bragg positions; and (c) difference profile.

TABLE 1
Comparative List of the Unit-Cell Parameters of $K_2MnF_5 \cdot H_2O$ Described in the Literature

a (Å)	6.04(1)	6.112(1)	6.000(2)	5.997(1)	5.881(1)
b (Å)	8.20(1)	8.120(2)	8.214(2)	8.120(1)	8.127(1)
c (Å)	5.94(1)	5.994(1)	6.123(2)	6.121(1)	6.259(1)
β(°)	96.5(2)	97.01(2)	96.93(2)	97.02(1)	96.35(1)
Ref.	(16)	(22)	(21)	this work	this work
Experimental techinque	XSCD	XPD	XSCD	NPD-295K	NPD-30K

Note. XSCD, X-ray single-crystal diffraction; XPD, X-ray powder diffraction; NPD, neutron powder diffraction. Space group $P2_1/m$ (no. 11).

Table 1 lists the cell parameters given in the literature for the room-temperature monoclinic phase of $K_2MnF_5 \cdot H_2O$. The structural determination by Edwards (18) and Molinier (7) was performed, in both cases, within the monoclinic space group $P2_1/m$ by single-crystal X-ray diffraction data analysis, and it led to very close atomic positions, except for the hydrogen position, which was not determined by Edwards. However, these structures differ from one another by the choice of the **a** and **c** monoclinic parameters. Edwards (18) proposed for $K_2MnF_5 \cdot H_2O$ a structure with the **a**-axis (6.04(1) Å) longer than the **c**-axis (5.94(1) Å), whereas Molinier proposed a structure with the **c**-axis (6.123(2) Å) longer than the **a**-axis (6.000(2) Å). Moreover, the values of these sets of cell parameters are quite different from each other.

Additionally, we have carried out an X-ray diffraction study on $K_2MnF_5 \cdot H_2O$ single crystals, which has revealed their natural tendency to grow as twinned crystals (27). This tendency is very probably at the origin of the difficulties found in establishing the correct cell parameters of $K_2MnF_5 \cdot H_2O$ from single-crystal diffractometer measurements. Precession images of a twinned crystal in the **a***c* plane can be interpreted as due to two superimposed reciprocal lattices rotated in such a manner that they match at each of the four **a*** levels. This corresponds to an angle of about 14°, which is just twice the value of (β-90). Due to the similarity between the a and c parameters, crystal packing defects based on their local interchange (eventually leading to local β angles of 83°) can be understood. This kind of defect would induce a local distortion of the cell that matches with the rest of the crystal in four cells in the **a** direction.

Cell parameters have been determined by refinement of neutron powder diffraction patterns recorded from 295 K down to 20 K. The profile-matching mode capability of the

FullProf program has been used in the $P2_1/m$ space group with the following possibilities: $a < c$ (labeled as *ac* model) and $c < a$ (labeled as *ca* model). A profile-matching procedure consists of the refinement of the full profile without requiring any structural model (28). The free parameters are the integrated intensities of all reflections generated from the space group symbol, peak shape, resolution function, and cell parameters (21). At 295 K profile-matching refinement of the neutron data using the $P2_1/m$ space group leads to close parameter values for the *ac model* ($a = 5.997(1)$, $b = 8.210(1)$, $c = 6.121(1)$ Å, and $\beta = 97.02(1)^\circ$) and the *ca model* ($a = 6.121(1)$, $b = 8.209(1)$, $c = 5.996(1)$ Å, and $\beta = 96.98(1)^\circ$). These values can be compared with those given in the literature (Table 1) and are very close to the cell parameters obtained by Molinier (7). Moreover, the introduction of the atomic positions in the Rietveld refinement leads us to conclude unambiguously on the validity of the model proposed by Molinier (7), i.e., the *ac model*, which will be used as reference for the following magnetic study.

The thermal evolution of the cell parameters between 295 and 20 K (Fig. 2) does not reveal any signature of first-order structural phase transition, but a change in the slopes can be detected in the temperature range 150–100 K. When the sample is cooled down to 20 K, the *a* and *c* parameters vary in opposite directions: the smaller parameter decreases while the larger one increases. This trend means that the small gap observed between the *a* and *c* values at room temperature becomes more important at low temperature. This fact, together with the twinning of the single crystals, explains the disagreement observed in the literature about the cell parameters.

The refinement of the high-resolution neutron data at low temperature ($T = 30$ K $> T_N$) leads to accurate determination of the atomic positions, including those of hydrogen atoms (Fig. 1). Table 2 shows the resultant atomic positions and some selected distances and angles in $K_2MnF_5 \cdot H_2O$. Only small changes in the atomic positions can be detected from this low-temperature refinement, compared to those determined at room temperature by single-crystal X-ray diffraction (7).

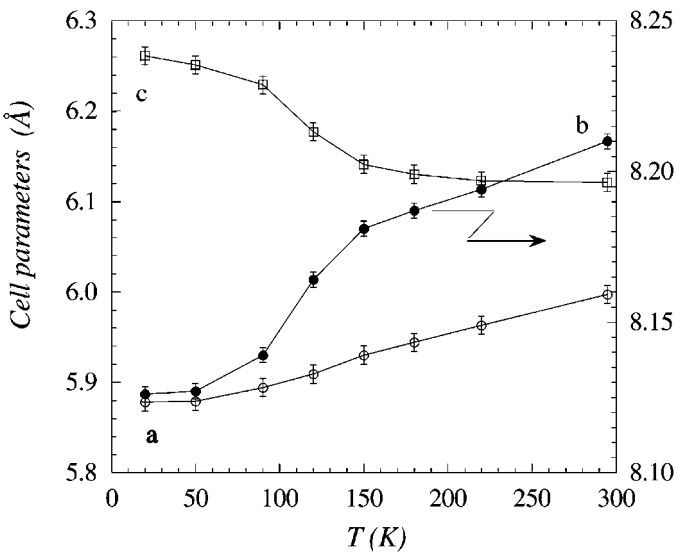

FIG. 2. Thermal variation of the cell parameters for $K_2MnF_5 \cdot H_2O$.

TABLE 2
Atomic Positions and Selected Distances (Å) and Angles (°) of $K_2MnF_5 \cdot H_2O$ from High-Resolution Neutron Data Refinement ($T = 30$ K; $\lambda = 2.3433$ Å)

Atom	Site	x	y	z	B (Å^2)
K1	2*e*	0.1047(15)	0.25	−0.4510(19)	1.88(25)
K2	2*e*	0.5001(17)	0.25	0.1207(16)	1.88(24)
Mn	2*a*	0	0	0	1.23(22)
F1	4*f*	0.1840(8)	0.0257(5)	0.2640(7)	2.29(12)
F2	4*f*	0.2540(8)	0.0324(5)	−0.1486(7)	2.51(14)
F3	2*e*	−0.0710(10)	0.25	−0.0106(12)	2.21(17)
O	2*e*	0.5867(11)	0.25	−0.4357(12)	1.64(15)
H	4*f*	0.6354(13)	0.1558(10)	−0.3688(11)	2.39(19)

Mn–F1 = 1.884(4)	Mn–F2 = 1.863(5)	Mn–F3 = 2.074(2)
F1–O[a] = 2.770(6)	F1–O[b] = 3.388(7)	
F2–O = 3.310(7)	F2–O[c] = 3.668(7)	
F1–K1[b] = 2.628(9)	F1–K1[d] = 3.117(8)	F1–K2 = 2.820(9)
F2–K2[a] = 2.708(7)	F2–K2 = 2.743(9)	F2–K1 = 2.666(10)

Mn–F1–K1[b] = 123.0(5)	F1[e]–K1–F2 = 87.3(4)	K1–F2–Mn = 103.2(5)
Mn–F2–K2 = 100.5(4)	F2[f]–K2–F2 = 74.6(3)	Mn–F2–K2[f] = 107.4(4)
Mn–F3–Mn = 156.9(1)		

[a] $1 - x, -1/2 + y, -z$.
[b] $x, y, 1 + z$.
[c] $1 - x, -1/2 + y, -1 - z$.
[d] $-x, -1/2 + y, -z$.
[e] $x, y, -1 + z$.
[f] $1 - x, -y, -z$.

The structure consists of chains of elongated (MnF_6) octahedra sharing, two *trans* corners, that are separated by the potassium atoms and the water molecules. The axial distortion, with four short Mn–F distances and two long ones, is due to the strong Jahn–Teller effect of the Mn(III) ion in a high-spin configuration $(t_{2g})^3 (e_g)^1$. The structure of $K_2MnF_5 \cdot H_2O$ can be considered as formed by infinite zig-zag chains of octahedra running parallel to the **b**-axis, with an intrachain Mn–F–Mn angle of 156.9(1)° at 30 K. The water molecules are connected to two neighbouring octahedra belonging to a same chain through O–H ⋯ F bonding. Potassium ions are located between the $(MnF_5)_n^{2n-}$ chains.

Magnetic Structure of $K_2MnF_5 \cdot H_2O$

The neutron powder diffraction pattern at 1.5 K (Fig. 3) shows several magnetic extra Bragg peaks, which cannot be

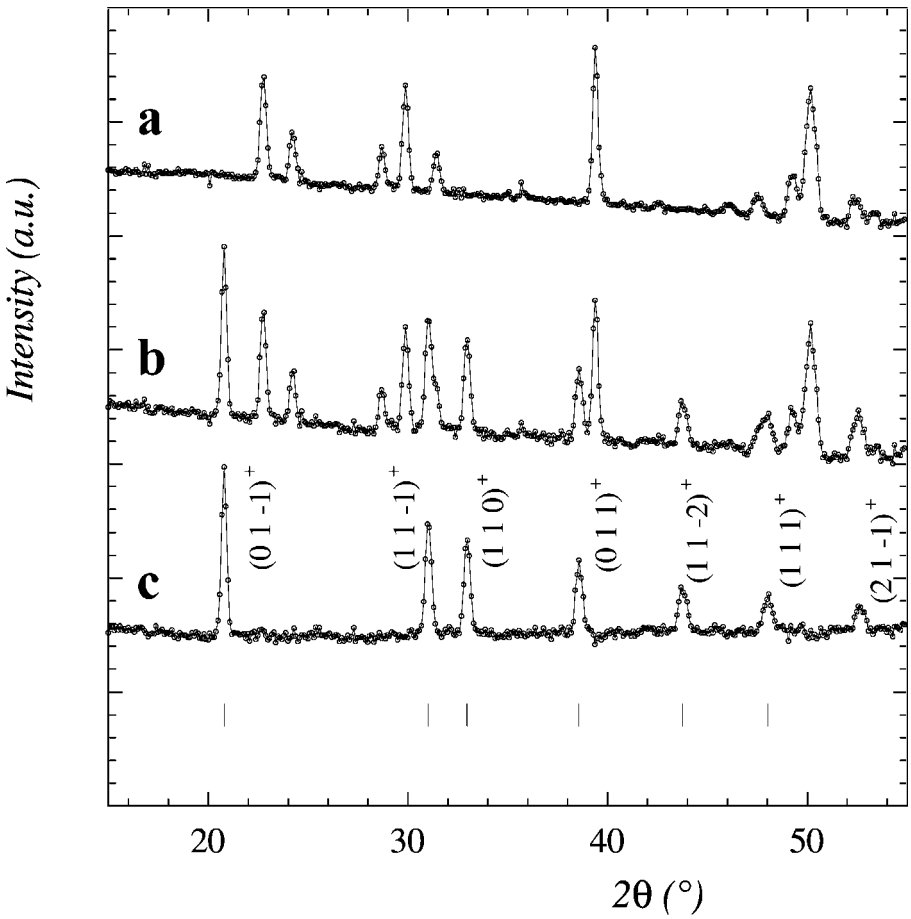

FIG. 3. Neutron patterns of $K_2MnF_5 \cdot H_2O$ ($\lambda = 2.426$ Å) at (a) 27 K and (b) 1.5 K. (c) Difference pattern and (d) positions of the observed magnetic Bragg peaks, from top, respectively.

indexed in the crystallographic cell but can be in a twofold cell ($\mathbf{a} \times \mathbf{b} \times 2\mathbf{c}$). These magnetic peaks can also be labeled as satellites of nuclear peaks with the propagation vector $\mathbf{k} = (0, 0, \frac{1}{2})$. Furthermore, the observed magnetic Bragg peaks follow the selection rule $k = 2n \pm 1$, which is the signature of the loss of the 2_1 screw axis. From a magnetic point of view, Mn_1 in (0 0 0) and Mn_2 in $(0\,\frac{1}{2}\,0)$ atomic positions are not equivalent (the screw axis becomes the antielement $2'_1$), leading to an antiferromagnetic ordering along the chains. The magnetic structure of $K_2MnF_5 \cdot H_2O$ is formed by antiferromagnetic chains coupled ferromagnetically along the **a**-axis and antiferromagnetically along the **c**-axis, as a consequence of the existence of the propagation vector $\mathbf{k} = \mathbf{c}^*/2$ (Fig. 4).

The magnetic manganese atoms occupy the Wyckoff site 2*a*, in the monoclinic unit cell of the $P2_1/m$ space group, on the symmetry center. Using Bertaut's macroscopic theory (29), we have obtained the irreducible representations of the space group $P2_1/m$ for the propagation vector $\mathbf{k} = (0, 0, \frac{1}{2})$ and determined the basis functions describing the possible magnetic structures (Table 3). The magnetic structure of $K_2MnF_5 \cdot H_2O$ is then consistent with the Γ_{2g} representation, with the restrictions $F_x = 0$ and $F_z = 0$, since the indexation of the observed magnetic reflections is consistent with a pure antiferromagnetic ordering along the chains (*y* axis). Existence of components along the *x* and *z* axes should induce the appearance of magnetic reflections with $k = 2n$, which have not been detected in the neutron powder diffraction patterns.

The thermal variation of the integrated intensity of the magnetic Bragg peaks is plotted in Fig. 5 and leads to a Néel temperature very close to 16.2(2) K, which is in relatively good agreement with the one obtained from magnetic susceptibility measurements (17.6 K) (6).

A Rietveld refinement of the neutron data at $T = 1.5$ K has been performed on the basis of the $\Gamma_{2g}(-)$ magnetic representation with $A_y \neq 0$, which is a collinear antiferromagnetic structure with the Mn^{3+} magnetic moment along the **b**-axis (Fig. 6). At 1.5 K, the magnetic moment per manganese atom, as determined from the model described

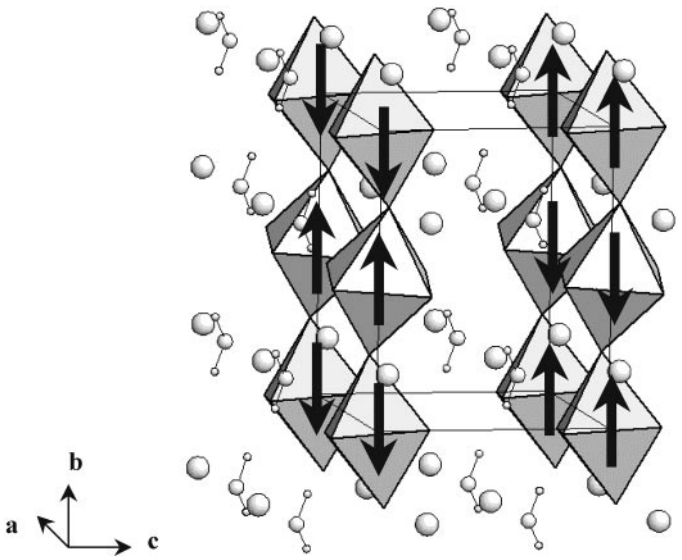

FIG. 4. Magnetic structure of $K_2MnF_5 \cdot H_2O$ [K atoms (large spheres), O atoms (medium spheres), and H atoms (small spheres)].

above, is equal to 3.1(1) μ_B, in agreement with those observed for other Mn(III) fluorides ($S = 2$) in a low-dimensional arrangement.

From previous studies on 3D magnetic structures of A_2MnF_5 (A = Rb) and $A_2MnF_5 \cdot H_2O$ (A = Rb, Tl) compounds, it has been established that the coupling between two Mn(III) atoms belonging to first-neighbor chains is antiparallel in the ordered magnetic state at low temperature, as it is for the intrachain coupling. This is obviously not the case for $K_2MnF_5 \cdot H_2O$.

In Table 4 we give the list of the effective exchange interactions that should be considered to study the problem. Within the chains, the major difference between $K_2MnF_5 \cdot H_2O$ and the Rb and Tl homologues lies in the difference observed in the Mn–F–Mn angles. Whereas the $(MnF_5)_n^{2n-}$ chains are almost linear in the Rb and in the Tl compounds, with Mn–F–Mn angles close to 180°, these chains are buckled in $K_2MnF_5 \cdot H_2O$, with an angle of 156.9(1)° at 30 K (163° at room temperature (7)). Such a configuration does not affect the magnetic coupling within the chains (J_1 in Table 4), which remains antiferromagnetic. But the magnitude of the exchange integral is reduced when the angle Mn–F–Mn is shifted from 180°, as has been observed for all homologues of the series and related compounds.

Concerning the interchain interactions, the exchange paths may involve the potassium atom orbitals. Figure 7 shows two exchange paths, involving K1 and K2 atoms, that correspond to the effective exchange interactions J_3 and J_2. In contrast with the fact that the **a** axis is shorter than the **c** axis, the distances between two Mn atoms through K atoms are indeed shorter in the **c** direction. There are two other exchange paths involving K1 and K2 atoms that are not shown in the figure, but they are given in Table 4 for the exchange integrals J_5 and J_4, respectively.

On another hand, additional exchange routes may involve water molecules, as shown by Massa in $Cs_2MnF_5 \cdot H_2O$ (30). For $K_2MnF_5 \cdot H_2O$ the water molecules are located in the plane supporting the short diagonal of the **ac** plane. This gives rise to two more exchange interactions, named J_6 and J_7 in Table 4. However, it should be noted that the corresponding distance is much longer than the Mn–F–K–F–Mn distances. It is then very likely that the exchange interactions verify $|J_1| \gg |J_2| \approx |J_3| > |J_4| \approx |J_5| \gg |J_6| \approx |J_7| \approx 0$. The sign of J_1 is clearly negative and it is responsible for the mode A and the $k_y = 0$ component of the

TABLE 3

Basic Functions of the Irreducible Representations of the Space Group $P2_1/m$ for the Propagation Vector $\mathbf{k} = (0\,0\,\frac{1}{2})$, Describing the Different Possible Magnetic Structures for $K_2MnF_5 \cdot H_2O$

	$\mathbf{k} = (0\,0\,\frac{1}{2})$		
	x	y	z
$\Gamma_{1g}(+)$	A_x	F_y	A_z
$\Gamma_{2g}(-)$	F_x	A_y	F_z

Note. The magnetic modes are defined as $\mathbf{F} = \mathbf{S}_1 + \mathbf{S}_2$ and $\mathbf{A} = \mathbf{S}_1 - \mathbf{S}_2$, where $\mathbf{S}_i$ ($i = 1, 2$) is the spin (axial vector) of the sublattice i for the ($2a$) Wyckoff position. The obtained representations are even with respect to the inversion operator and denoted Γ_g. The character of the 2_{1y} screw axis generator is given in parentheses.

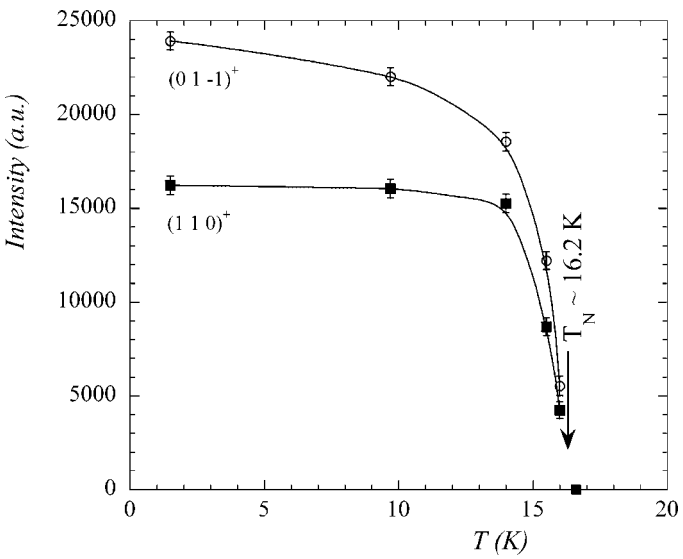

FIG. 5. Thermal variation of the integrated intensity of the $(0\,1\,\bar{1})^+$ and $(1\,1\,0)^+$ magnetic Bragg peaks. The continuous lines are only guides for the eyes.

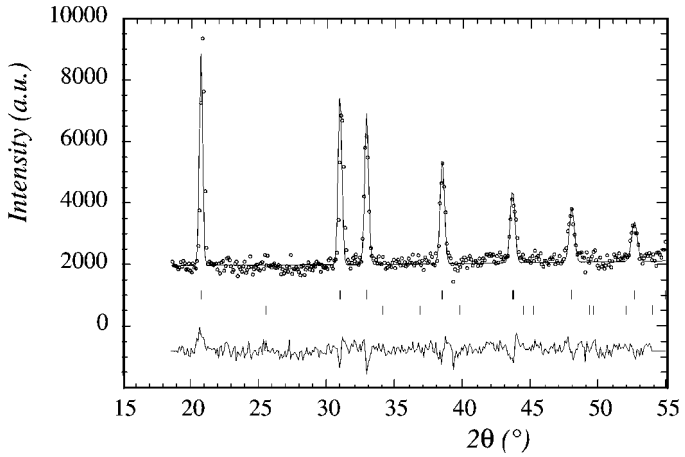

FIG. 6. $K_2MnF_5 \cdot H_2O$ neutron diffraction magnetic patterns at 1.5 K: (upper profile) experimental points (circles) and calculated (continuous line) (lower profile) difference profile; upper vertical ticks are for 2θ Bragg positions (mode A_y) and lower vertical ticks are for extra Bragg peak positions due to F_x and F_z ferromagnetic components.

propagation vector. We shall discard the two weakest interactions (J_6 and J_7) in the following.

In our case, there is no magnetic phase transition below T_N, so the first ordered state is the ground state. We can use the method of (31) to evaluate the conditions to be satisfied by the exchange integrals in order to have the propagation vector $\mathbf{k} = (0, 0, \frac{1}{2})$ as the ground state. The first ordered state is obtained, as a function of $\mathbf{k}$ (on the surface or in the interior of the Brillouin zone) and the exchange integrals, as the eigenvector corresponding to the lowest eigenvalue of the negative Fourier transform of the exchange integral matrix:

$$\xi_{ij}(\mathbf{k}) = -\sum_{\mathrm{m}} J_{ij}(\mathbf{R}_{\mathrm{m}}) \cdot \exp\{-2\pi i\, \mathbf{k}\mathbf{R}_{\mathrm{m}}\}. \qquad [1]$$

The indices i, j refer to the magnetic atoms in a primitive cell, $J_{ij}(\mathbf{R}_{\mathrm{m}})$ is the isotropic exchange interaction between the spins of atoms i and j in unit cells separated by the lattice vector $\mathbf{R}_{\mathrm{m}}$. We have adopted the interaction energy between two spins as

$$W = -J_{ij}\mathbf{S}_i\mathbf{S}_j = -J_{ij}S_iS_j\mathbf{s}_i\mathbf{s}_j = -J_{ij}\mathbf{s}_i\mathbf{s}_j, \qquad [2]$$

so $J_{ij}(\mathbf{R}_{\mathrm{m}})$ includes the spin modules and $\mathbf{s}_i$ is a unit vector. This is not the same convention used in Ref. (28), where the minus sign is not given. Our convention agrees with the common use of negative J for antiferromagnetic coupling. In our case, there are only two magnetic atoms of the same chemical species (Mn^{3+}, $S = 2$) per primitive cell, so Eq. [1] is a 2×2 hermitian matrix. Considering the isotropic exchange interactions up to a distance of 7.5 Å, given in Table 4, the terms of the matrix are

$$\xi_{11}(\mathbf{k}) = \xi_{22}(\mathbf{k}) = -2(J_2 \cos 2\pi X + J_3 \cos 2\pi Z) \qquad [3]$$

$$\xi_{12}(\mathbf{k}) = \xi_{21}(\mathbf{k})^* = -(J_1 + 2J_4 \cos 2\pi X + 2J_5 \cos 2\pi Z)(1 + \exp\{2\pi i Y\}).$$

The energy (lowest eigenvalue) as a function of the exchange integrals and $\mathbf{k} = (X, Y, Z)$ is

$$\lambda(\mathbf{k}) = -\mathbf{2}(J_2 \cos 2\pi X + J_3 \cos 2\pi Z) + (J_1 + 2J_4 \cos 2\pi X + 2J_5 \cos 2\pi Z)\{2(1 + \cos 2\pi Y)\}^{1/2}. \qquad [4]$$

The vector $\mathbf{k}$ minimizing $\lambda(\mathbf{k})$ for a given set of J_{ij} is the propagation vector of the magnetic structure, and the spin configuration is obtained from the corresponding eigenvector. To simplify the discussion we shall assume that the

TABLE 4
List of Exchange Integrals and Conditions for the Different Propagation Vectors to be the Ground State for Mode *A*

Exchange integrals	Representative atom positions	Number of equivalent Mn^{3+} ions	Distance (Å)	Exchange paths
J_1	$(0,0,0) \leftrightarrow (0,1/2,0)$	2	4.06	super-exchange: Mn–F3–Mn (156.9°), strongest
J_2	$(0,0,0) \leftrightarrow (1,0,0)$	2	5.88	super-super-exchange: Mn–F–K2–F–Mn
J_3	$(0,0,0) \leftrightarrow (0,0,1)$	2	6.26	super-super-exchange: Mn–F–K1–F–Mn
J_4	$(0,0,0) \leftrightarrow (1,1/2,0)$	4	7.15	super-super-exchange: Mn–F–K2–F–Mn
J_5	$(0,0,0) \leftrightarrow (0,1/2,1)$	4	7.46	super-super-exchange: Mn–F–K1–F–Mn
J_6	$(0,0,0) \leftrightarrow (1,0,1)$	2	8.10	super-super-exchange: Mn–F1–O–F1–Mn
J_7	$(0,0,0) \leftrightarrow (-1,0,1)$	2	9.04	super-super-exchange: Mn–F2–O–F2–Mn

Propagation vector ($Y = 0$; $X, Z = 0, \frac{1}{2}$)	Conditions on J ($J_6 = J_7 = 0$)
$\mathbf{k} = (0,0,0)$	$2J_4 < J_2$ and $2J_5 < J_3$
$\mathbf{k} = (1/2,0,1/2)$	$2J_4 > J_2$ and $2J_5 > J_3$
$\mathbf{k} = (1/2,0,0)$	$2J_4 > J_2$ and $2J_5 < J_3$
$\mathbf{k} = (0,0,1/2)$	$2J_4 < J_2$ and $2J_5 > J_3$

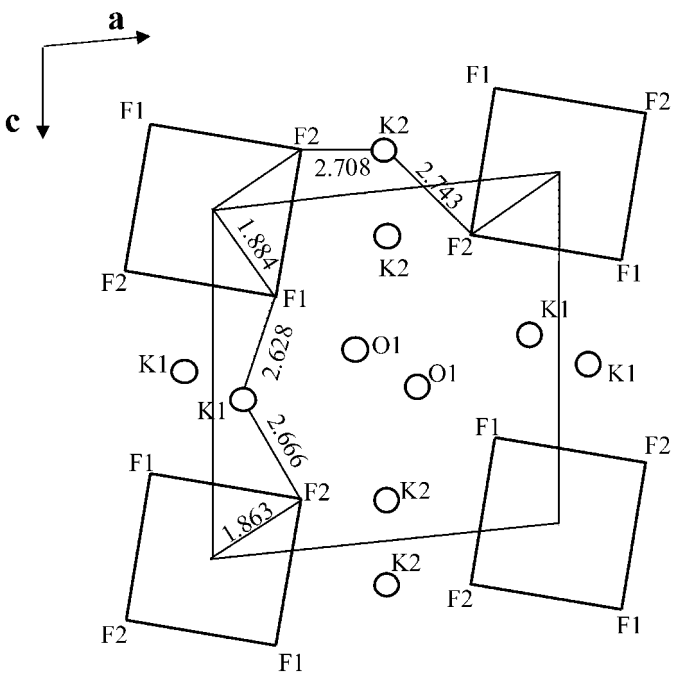

FIG. 7. Two Mn–Mn pathways for $K_2MnF_5 \cdot H_2O$ involving K atoms along the **a** and **c** axes in the *ac* plane (bond distances expressed in Å).

propagation vector has $Y = 0$, because the strongest interaction J_1 along the chains, e.g., Mn(1) at (000) and Mn(2) at $(0\ \frac{1}{2}\ 0)$, is negative and the periodicity along **b** should be conserved. The energy can then be written for $\mathbf{k} = (X, 0, Z)$ as

$$\lambda(\mathbf{k}) = 2\{J_1 + (2J_4 - J_2)\cos 2\pi X + (2J_5 - J_3)\cos 2\pi Z\}. \quad [5]$$

Taking the gradient of $\lambda(\mathbf{k})$ with respect to **k** equal to zero, it is very simple to demonstrate that the only conditions for the maximum or minimum of $\lambda(\mathbf{k})$ are $X = 0, \frac{1}{2}$, and $Z = 0, \frac{1}{2}$. The stability conditions of the different magnetic structures with $Y = 0$ are given in Table 4; they are obtained from the Hessian matrix of (5) and are definitely positive. We see that the observed propagation vector of $K_2MnF_5 \cdot H_2O$, $\mathbf{k} = (0, 0, 1/2)$, is stable for $2J_4 < J_2$ and $2J_5 > J_3$. So this structure is the ground state, even in the case where all interactions are negative, provided the conditions are realized. In the case where all interactions are negative the conditions are rewritten as: $2|J_4| > |J_2|$ and $2|J_5| < |J_3|$, and we may consider the super-super-exchange paths involving Mn(000)–F1, F2–K2–F1, F2–Mn(100) (and equivalent) "frustrated" in the sense that the coupling is "ferromagnetic" and the corresponding effective exchange integral is "negative." However, as we have shown, the important point is the total energy minimization and the conditions $2|J_4| > |J_2|$ is sufficient to get the observed magnetic structure.

It is expected that for the weak super-super-exchange interactions subtle details of the structural changes may result in a change of sign of some effective exchange integrals; it may be possible (even if unlikely) that J_2 becomes positive. This could accomplished by a weak overlap, due to the buckling of octahedra and through F and K-atoms, of the t_{2g} and d_{z2} half-filled orbitals of Mn^{3+} with the empty $d_{x^2-y^2}$ orbitals in an adjacent position. In such a case all exchange "bonds" are satisfied.

CONCLUDING REMARKS

The crystal structure of $K_2MnF_5 \cdot H_2O$ has been reexamined by neutron powder diffraction, which has allowed to determine unambiguously that the correct structure is the one with a set of unit-cell parameters having $c > a$ in the $P2_1/m$ space group.

The magnetic structure of $K_2MnF_5 \cdot H_2O$ has been determined: (i) intrachain antiferromagnetic interactions are dominant in agreement with analogous fluoromanganates; (ii) interchain magnetic effective coupling is antiferromagnetic in the **c** direction, $\mathbf{k} = (0, 0, 1/2)$, and ferromagnetic in the **a** direction. The magnetic moment for the Mn(III) atoms is found to be equal to 3.1(1) μ_B at 1.5 K. We have proved that we do not need to have ferromagnetic (positive) exchange interactions in order to get the observed structure as the ground state of a *classical* Heisenberg Hamiltonian.

Nevertheless, two important aspects deserve to be studied in more detail: (a) the origin of the important change occurring in the unit-cell constants at low temperature (simultaneous decrease of *a* and *b* cell parameters and increase of the *c* parameter); and (b) the quantitative values of the exchange integrals. This cane only be obtained experimentally from an inelastic neutron scattering experiment on single crystals by fitting the spin wave dispersion relations, or by *ab initio* electronic structure calculations.

ACKNOWLEDGMENTS

One of us (P.N.) thanks the "Training and Mobility of Researchers—Access to Large-Scale Facilities (TMR-LSF)" program of the European Union for financial support during the stay at LLB.

REFERENCES

1. P. Núñez, J. Darriet, P. Bukovec, A. Tressaud, and P. Hagenmuller, *Mater. Res. Bull.* **22,** 661 (1987).
2. J. Pebler, W. Massa, H. Lass, and B. Ziegler, *J. Solid State Chem.* **71,** 87 (1987).
3. (a) P. Núñez, A. Tressaud, J. Darriet, P. Hagenmuller, W. Massa, S. Kummer, and D. Babel, *J. Solid State Chem.* **77,** 240 (1988); (b) P. Núñez, A. Tressaud, W. Massa, D. Babel, A. Boireau, and J. L. Soubeyroux, *Phys. Status Solidi* **A127,** 505 (1991).
4. P. Núñez, A. Tressaud, J. Darriet, P. Hagenmuller, G. Hahn, G. Frenzen, W. Massa, D. Babel, A. Boireau, and J. L. Soubeyroux, *Inorg. Chem.* **31,** 770 (1992).

5. M. Molinier, C. Frommen, W. Massa, J. Pebler, and T. Roisnel, *Z. Naturf.* **48a,** 1054 (1993).
6. M. Andrés, Thesis, University of Zaragoza, Spain, 1988; F. Palacio and M. C. Morón, *in* "Research Frontiers in Magneto Chemistry" (C. J. O'Connor, Ed.), p. 227. Academic Press, Orlando, 1993.
7. M. Molinier, Thesis, University of Marburg, 1993.
8. (a) P. Núñez, T. Roisnel, and A. Tressaud, *Solid State Commun.* **92**(7), 601 (1994); (b) P. Núñez, T. Roisnel, *J. Solid State Chem.* **124,** 338 (1996).
9. M. Steiner, M. Winkelmann, M. Baehr, D. Hohlwein, A. Krimmel, C. Frommen, M. Mangold, and J. Pebler, *Physica B* **241–243,** 555 (1998).
10. J. Pebler, C. Frommen, M. Mangold, and W. Treutmann, *Z. Naturforsch* **54a,** 317 (1999).
11. P. Köhler, W. Massa, D. Reinen, B. Hoffmann, and R. Hoppe, *Z. Anorg. Allg. Chem.* **446,** 131 (1978).
12. F. Rodriguez, P. Núñez, and M. C. Marco de Lucas, *J. Solid State Chem.* **110,** 370 (1994).
13. P. Núñez, C. Elias, J. Fuentes, X. Solans, A. Tressaud, M. C. Marco de Lucas, and F. Rodriguez, *J. Chem. Soc. Dalton Trans.*, 4335 (1997).
14. T. Roisnel, P. Núñez, W. Massa, and A. Tressaud, *Physica B* **234–236,** 579 (1997).
15. M. E. Fischer, *Am. J. Phys.* **32,** 343 (1964).
16. T. Smith and S. A. Friedberg, *Phys. Rev.* **176,** 660 (1968).
17. G. Palmer, *in* 'Experimental Inorganic Chemistry," p. 479. Cambridge University Press, Cambridge, UK, 1954.
18. A. J. Edwards, *J. Chem. Soc.* **A,** 2653 (1971).
19. P. Bukovec, B. Orel, and J. Siftar, *Monast. Chem.* **105,** 1299 (1974).
20. T. Roisnel, J. Rodriguez-Carvajal, M. Pinot, G. André, and F. Bourée, *Mater. Sci. Forum* **166–169,** 245 (1994).
21. J. Rodriguez-Carvajal, "Abstracts of the Satellite Meeting on Powder Diffraction of the XV Congress of the IUcr," p. 127, Toulouse, France, 1991.
22. V. F. Sears, *Neutron News* **3**(3)**,** 26 (1992).
23. P. J. Brown, *in* "International Tables for Crystallography," (A. J. C. Wilson, Ed.), Vol. C, Table 4.4.4. Kluwer, Dordrecht, 1993.
24. J. R. Günter, J. P. Matthieu, and H. R. Oswald, *Helv. Chim. Acta* **61,** 328 (1978).
25. P. Bukovec and V. Kaûcic, *Acta Crystallogr.* **B34,** 3339 (1978).
26. V. Kaûcic and P. Bukovec, *Acta Crystallogr.* **B34,** 3337 (1978).
27. F. Palacios and E. Molins, personal communications. [In the present case, twinned and single crystals were produced in the same batch. Their separation was done under the microscope, by classifying the crystals by their darkness degree.]
28. A. Le Bail, H. Duroy, and J. F. Fourquet, *Mater. Res. Bull.* **23,** 447 (1988).
29. E. F. Bertaut, *Acta Crystallogr.* **A24,** 217–231 (1968); E. F. Bentaut, *in* "Magnetism" (G. T. Rado and H. Suhl, Eds.), Vol. 3, p. 150. New York Academy, 1963.
30. F. Hahn and W. Massa, *Z. Naturforsch.* **45b,** 1341 (1990).
31. M. J. Freiser, *Phys. Rev.* **123,** 2003 (1961).